1-1-2012

Effect of iron content on sintering behavior of Ti-V-Fe-Al near-beta titanium alloy

Dmytro G. Savvakin
National Academy of Sciences, Ukraine

Andrew Carman
University Of Wollongong, acarman@uow.edu.au

Orest M. Ivasishin
National Academy of Sciences, Ukraine

Mykhailo V. Matviychuk
National Academy of Sciences, Ukraine

Azdiar A. Gazder
University of Wollongong, azdiar@uow.edu.au

See next page for additional authors

Effect of iron content on sintering behavior of Ti-V-Fe-Al near-beta titanium alloy

Abstract

Two near-beta Ti-10V-3Fe-3Al and Ti-10V-2Fe-3Al alloys were produced by blended elemental powder metallurgy using hydrogenated titanium and V-Fe-Al master alloy powders. The distributions of the alloying elements were investigated at different stages of transformation of the heterogeneous powder compacts into the final homogeneous alloy product. The influence of iron content on chemical homogenization, densification, microstructure, and mechanical properties of as-sintered alloys was discussed with respect to the fast diffusion mobility of iron in titanium. It was concluded that a 1 pct increase in Fe content, as the alloying element with the fastest diffusivity in titanium, has a positive effect on densification. However, this also results in some grain coarsening of the final material. The attained mechanical properties were comparable with those of cast/wrought near-beta titanium alloys.

Keywords

effect, ti, iron, v, fe, al, near, beta, titanium, alloy, content, sintering, behavior

Publication Details

Savvakin, D. G., Carman, A., Ivasishin, O. M., Matviychuk, M. V., Gazder, A. A. & Pereloma, E. V. (2012). Effect of iron content on sintering behavior of Ti-V-Fe-Al near-beta titanium alloy. Metallurgical and Materials Transactions A: Physical Metallurgy and Materials Science, 43 (2), 716-723.

Authors

Dmytro G. Savvakin, Andrew Carman, Orest M. Ivasishin, Mykhailo V. Matviychuk, Azdiar A. Gazder, and Elena V. Pereloma

Effect of Iron Content on Sintering Behavior of Ti-V-Fe-Al Near-β Titanium Alloy

DMYTRO G. SAVVAKIN, ANDREW CARMAN, OREST M. IVASISHIN, MYKHAILO V. MATVIYCHUK, AZDIAR A. GAZDER, and ELENA V. PERELOMA

Two near-β Ti-10V-3Fe-3Al and Ti-10V-2Fe-3Al alloys were produced by blended elemental powder metallurgy using hydrogenated titanium and V-Fe-Al master alloy powders. The distributions of the alloying elements were investigated at different stages of transformation of the heterogeneous powder compacts into the final homogeneous alloy product. The influence of iron content on chemical homogenization, densification, microstructure, and mechanical properties of as-sintered alloys was discussed with respect to the fast diffusion mobility of iron in titanium. It was concluded that a 1 pct increase in Fe content, as the alloying element with the fastest diffusivity in titanium, has a positive effect on densification. However, this also results in some grain coarsening of the final material. The attained mechanical properties were comparable with those of cast/wrought near-beta titanium alloys.

DOI: 10.1007/s11661-011-0875-9

I. INTRODUCTION

THE β titanium alloys possess the highest strength-to-weight ratio among all titanium grades, making them attractive as constructional materials for emerging applications, such as load-bearing components in the aviation industry.[1] Despite a unique combination of high specific strength and excellent corrosion resistance, the application of titanium alloys, including β titanium alloys, is significantly restricted by the high cost of the titanium itself, the high cost of component manufacture, and the considerable material waste during machining.

To produce titanium parts in a more cost-effective manner, near-net-shape powder metallurgy processing can be successfully used.[2–4] Blended elemental powder metallurgy (BEPM) is one of the most cost-effective manufacturing routes among the powder technologies.[4–8] In this approach, the alloying elements are added to titanium as elemental or master alloy powders. This allows for ''tailoring'' of the compositions and microstructural features, which is more difficult to achieve using the traditional ingot route. In addition, the need for machining the near-net shape components may be minimized. The synthesis of titanium alloys using BEPM involves several diffusion-controlled processes such as the chemical homogenization of heterogeneous powder compacts, their densification, and the corresponding microstructural evolution (*i.e.*, grain growth and the formation of a uniform microstructure). The chemical homogeneity, fine-grained microstructure, and high relative density (close to 98 to 99 pct) associated with titanium products synthesized by BEPM leads to mechanical properties that meet the standards of industrial applications as they are comparable with corresponding cast/wrought alloys.

Beta Ti-10V-2Fe-3Al (wt pct) alloy is widely used in aviation for the fabrication of large load-bearing components because of its high strength, good fracture toughness, and deep hardenability.[9] This composition has also been produced by BEPM[10] using hydrogenated titanium as the base powder to accelerate diffusion and to improve synthesis.[11] Despite obtaining a reasonably good combination of properties in a sintered Ti-10V-2Fe-3Al alloy, its BEPM processing has revealed the specific peculiarities of powder compact homogenization and shrinkage, which led to significant difficulties in achieving the desired density of 98 pct.

Since the high diffusivity of Fe in titanium enhances the sinterability of titanium alloys,[12,13] increasing the Fe content can improve the density and other diffusion-controlled characteristics of complex titanium compositions produced by BEPM. In the present work, a modified Ti-10V-2Fe-3Al (Ti-1023) alloy with a 1 pct increase in Fe content (*i.e.*, Ti-10V-3Fe-3Al, Ti-1033 composition) was sintered by BEPM. The aim of this study was to conduct a detailed investigation of the sintering behavior of the Ti-10V-3Fe-3Al alloy in order to compare and contrast the BEPM processing and the characteristics of the final product with those of the Ti-1023 alloy.

DMYTRO G. SAVVAKIN, Senior Researcher, and OREST M. IVASISHIN, Deputy Director, are with the Institute for Metal Physics, National Academy of Sciences Ukraine, UA-03142 Kiev, Ukraine. ANDREW CARMAN, Associate Research Fellow, AZDIAR A. GAZDER, Research Fellow, and ELENA V. PERELOMA, Professor, are with the School of Mechanical, Materials & Mechatronic Engineering, University of Wollongong, Wollongong, NSW 2522, Australia. Contact e-mail: elenap@uow.edu.au MYKHAILO V. MATVIYCHUK, formerly with the Institute for Metal Physics, National Academy of Sciences, is now with ADMA Products, Inc., Hudson, OH 44236.

Manuscript submitted March 14, 2011.
Article published online September 8, 2011

II. EXPERIMENTAL

The base hydrogenated titanium powder had a particle size <100 μm and contained 3.5 wt pct hydrogen. A complex master alloy with 62.5 pct V-18.75 pct Fe-18.75 pct Al composition was produced by vacuum arc remelting. It was then milled into powder <40 μm and blended with the base powder in the necessary ratio to reach the Ti-1033 composition. The powder blend obtained was die-pressed at room temperature under a load of 640 MPa to form green compacts (cylindrical pellets of Ø10-mm diameter and 12-mm length or rectangular bars of $10 \times 10 \times 70$ mm^3). Similarly, a powder blend corresponding to the Ti-1023 alloy composition was also produced and die pressed using a 66.7 pct V-13.3 pct Fe-20.0 pct Al complex master alloy powder. The powder compacts were subsequently heated under vacuum using selected time–temperature regimes for dehydrogenation and alloy synthesis. Processing was interrupted at the following points in the sintering schedule and samples were produced for microstructural analysis:

(a) Step I: heating to 1293 K (1020 °C), immediate furnace cooling
(b) Step II: 1293 K (1020 °C) for 15 minutes, heating to 1523 K (1250 °C), immediate furnace cooling
(c) Step III: 1293 K (1020 °C) for 15 minutes + 1523 K (1250 °C) for 4 hours, furnace cooling

The heating rate was 280 K to 283 K (7 °C to 10 °C) / min^{-1} for all heating steps. A holding stage of 15 minutes at 1293 K (1020 °C) before additional heating to the sintering temperature of 1523 K (1250 °C) was used to avoid the possible formation of eutectic concentrations in the Ti-Fe system, as the formation of eutectic melts leads to excessive porosity.[14]

An ELTRAOH900 gas analyzer (ELTRA GmbH Company, Neuss, Germany) was used to determine the initial and final hydrogen contents in the material. High-temperature dilatometry was used to study shrinkage behavior upon continuous heating at 280 K min^{-1} (7 °C min^{-1}) to 1523 K (1250 °C). The density of the samples at the final sintering stage was determined by the Archimedes method. The residual porosity was measured by image analysis of polished cross sections using an Olympus* IX70 light microscope. Metallographic sample preparation for optical observations was carried out using standard techniques. The specimen surfaces were etched with Kroll's solution (2 mL HF, 5 mL HNO_3, and 93 mL H_2O) to reveal the microstructure.

A detailed microstructural and compositional analysis of the Ti-1033 alloy was performed using a JEOL JSM 7001F (JEOL, Tokyo, Japan) field emission-scanning electron microscope equipped with a Bruker**-AXS XFlash detector energy-dispersive X-ray (EDX) analysis system. An accelerating voltage of 15 kV was used, and the probe current was selected to provide an EDX count rate of approximately 25 kcps to ensure good statistics. Both elemental X–ray mapping and X–ray line scans were carried out on the samples using standardless quantification techniques.

Tensile testing of final synthesized alloys was conducted at room temperature following the ASTM E8M-04 specification using round specimens of Ø4-mm diameter and 20-mm gage length.

*Olympus is a trademark of Olympus Corporation, Tokyo, Japan.

**Brucker is trademark of Brucker Corporation, Billerica, MA.

III. RESULTS

During synthesis, the following processes take place: chemical homogenization, densification, and microstructure evolution. For both studied compositions, all these processes started and developed to different degrees by heating Step I. Although this article mainly focuses on the study of Ti-1033, more details on the Ti-1023 alloy are given elsewhere.[10]

Dehydrogenation of the base hydrogenated powder under vacuum occurs when it is heated above 573 K (300 °C) and is completed by Step I. It is accompanied by significant shrinkage of the powder compacts, which is observed during continuous heating between 573 K and 1073 K (300 °C and 800 °C) (Figure 1). The shrinkage rate decreases at the final stage of dehydrogenation and then increases again above 1173 K (900 °C) at the start of powder particle sintering. Comparison of the shrinkage behaviors of the Ti-1033 and Ti-1023 compositions shows that shrinkage of the former compact is more pronounced at temperatures above 873 K (600 °C).

Despite the fact that the sintering process starts within the temperature range corresponding to Step I, it is at an early stage as evidenced by the significant amount of residual porosity and the nonuniform distribution of alloying elements in the microstructure (Figure 2). Diffusion of the alloying elements (Fe, Al, and V) from

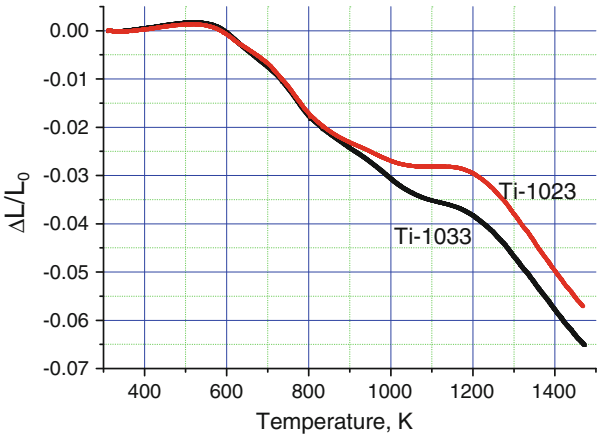

Fig. 1—Dilatometric curves of Ti-1033 and Ti-1023 BEPM compacts based on hydrogenated titanium.

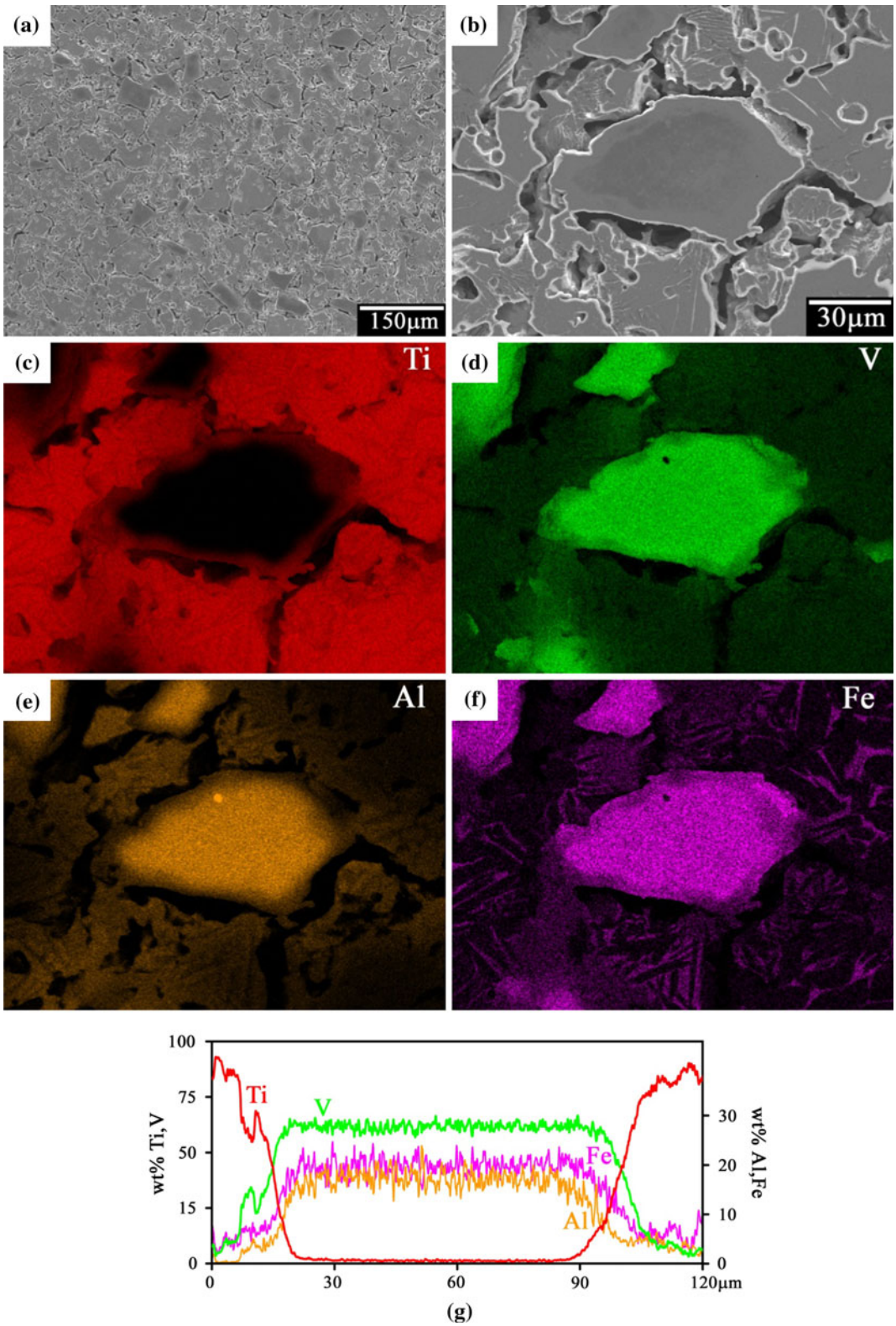

Fig. 2—Microstructure of Ti-1033 compact after Step I processing at low (*a*) and high (*b*) magnifications together with (b) corresponding to (b) X-ray maps of (*c*) Ti, (*d*) V, (*e*) Al, (*f*) Fe, and (*g*) line scan across the powder particle.

the master alloy particles into the titanium matrix has only just started (Figure 2), creating considerable concentration gradients of these elements and corresponding microstructural inhomogeneity. As shown in Figures 2(d) through (f) for the Ti-1033 composition, the diffusion of Fe in the Ti matrix is more advanced,

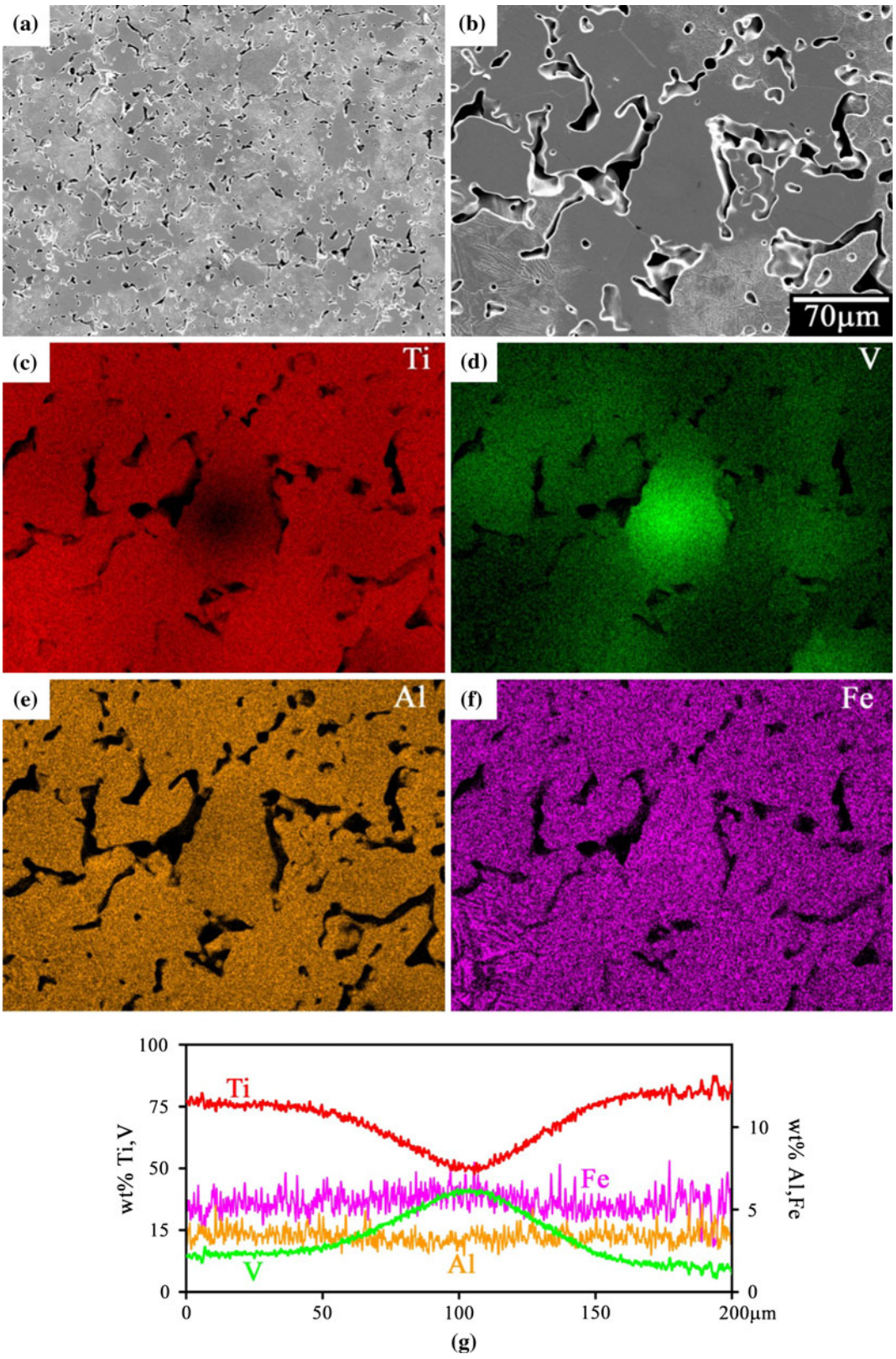

Fig. 3—Microstructure of Ti-1033 compact after Step II processing at low (*a*) and high (*b*) magnifications together with (b) corresponding to X-ray maps of (*c*) Ti, (*d*) V, (*e*) Al, (*f*) Fe, and (*g*) line scan across the powder particle.

followed by Al. Contrarily, V remains concentrated within the master alloy particles with a clearly outlined interface between the particle and the matrix. The microstructure of the sample is nonuniform, including nonlamellar α and lamellar $\alpha + \beta$ areas of titanium matrix and undissolved alloying particles (Figure 2(b)).

Step II is characterized by the development of chemical homogenization and densification. The characteristic features of these processes for the Ti-1033 composition are shown in Figure 3. The portion of lamellar $\alpha + \beta$ structure has increased in comparison with the previous stage, whereas remnants of the alloying particles have mostly disappeared. A homogeneous distribution of Al and Fe in the titanium matrix was achieved during this sintering step. Although V is more uniformly distributed in the matrix compared with the previous Step I condition, some remaining powder particles are still enriched in V (Figure 3(d)). This finding is supported by the concentration profiles in Figure 3(g), which also show that Al and Fe are completely homogenized between the particles and the matrix. The size and total volume fraction of pores was noticeably reduced at this stage. Moreover, pore morphology has changed from the initial non-irregular, elongated shape to a more spherical shape.

Synthesis of both Ti-1033 and Ti-1023 compositions was complete by Step III. The fully homogeneous redistribution of all alloying elements into the titanium matrix was achieved with a corresponding uniform microstructure (Figure 4). The microstructures of both alloys are similar and consist of relatively fine β grains with precipitation of α lamellae within them. The Ti-1033 alloy was characterized with an average β grain size of 145 μm and fine intragrain α-phase lamellae. The grain size of the Ti-1023 alloy was much smaller (105 μm) with thicker α-phase lamellae. Despite the fact that the porosity of the compacts decreased markedly during the final sintering step, fine residual pores with a near spherical shape are present in the microstructures. The density of the synthesized Ti-1033 alloy was determined to be 4.52 ± 0.005 gm cm^{-3} with a residual porosity of 3.4 vol pct, whereas the Ti-1023 composition contained a slightly higher residual porosity of 4 pct. A safe level of hydrogen content in the final alloys was also attained at $\leq$0.002 to 0.003 pct. The synthesized Ti-1033 material after furnace cooling exhibits good strength characteristics but poor ductility (Table I).

For comparison, the Ti-1023 alloy synthesized by the same time–temperature regime has noticeably lower strength but better ductility.

IV. DISCUSSION

Differences were noted in the sintering behavior and final properties of the Ti-1033 and Ti-1023 alloys produced by similar processing steps via BEPM. All of these differences can be attributed to the difference in iron content, as all other processing and compositional parameters were constant. First, the difference in shrinkage behavior for the two noted compositions is clearly shown in Figure 1. This distinction occurred at

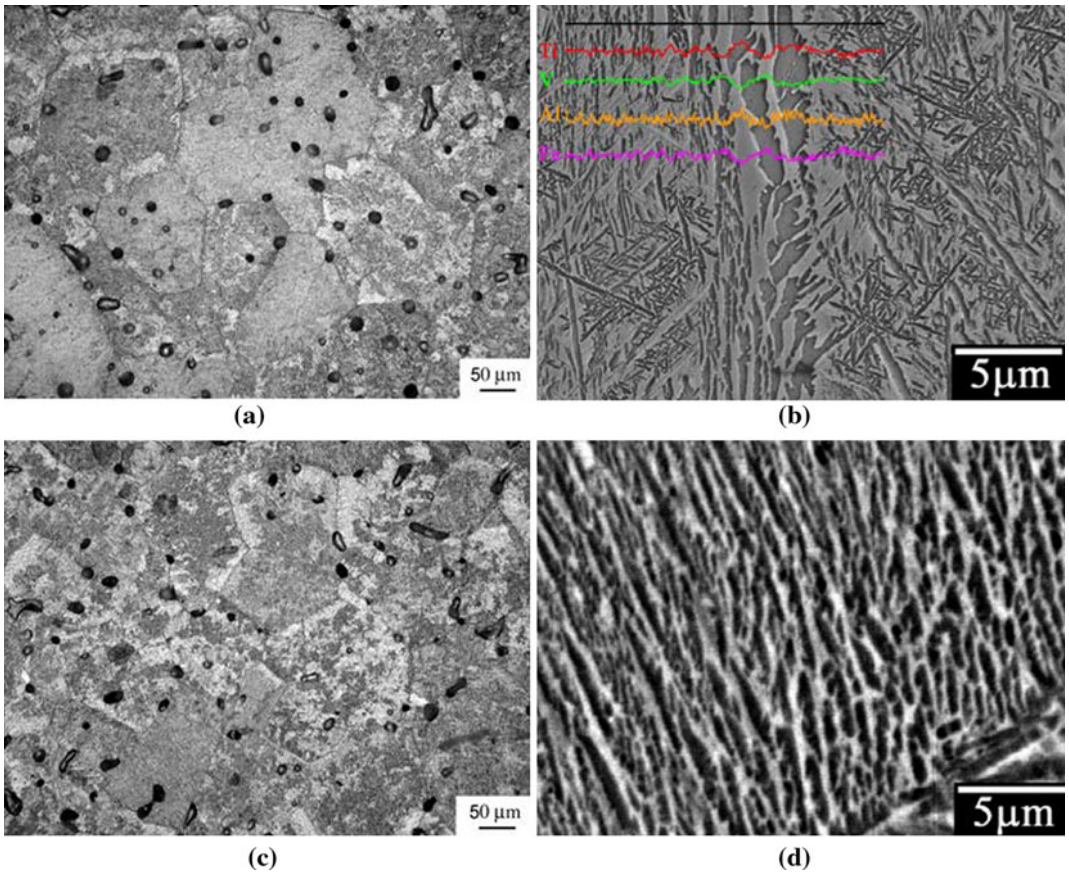

Fig. 4—Optical micrographs of synthesized Ti-1033 (*a*) and Ti-1023 (*c*) alloys and SEM micrographs of Ti-1033 (*b*) with its corresponding concentration profiles and Ti-1023 (*d*) alloys.

Table I. Properties of Synthesized Alloys (After Step III)

Alloy	Residual Porosity (pct)	Grain Size (μm)	YS* (MPa)	UTS† (MPa)	El.‡ (pct)	RA§ (pct)
Ti-1033	3.4 ± 0.2	145 ± 40	984 ± 57	1133 ± 4	1.7 ± 0.4	7 ± 0.6
Ti-1023	4.0 ± 0.2	105 ± 32	944 ± 18	1033 ± 5	8.0 ± 1.2	13.5 ± 2.5

*YS is yield strength.
†UTS is ultimate tensile strength.
‡El. is total elongation.
§RA is reduction in area.

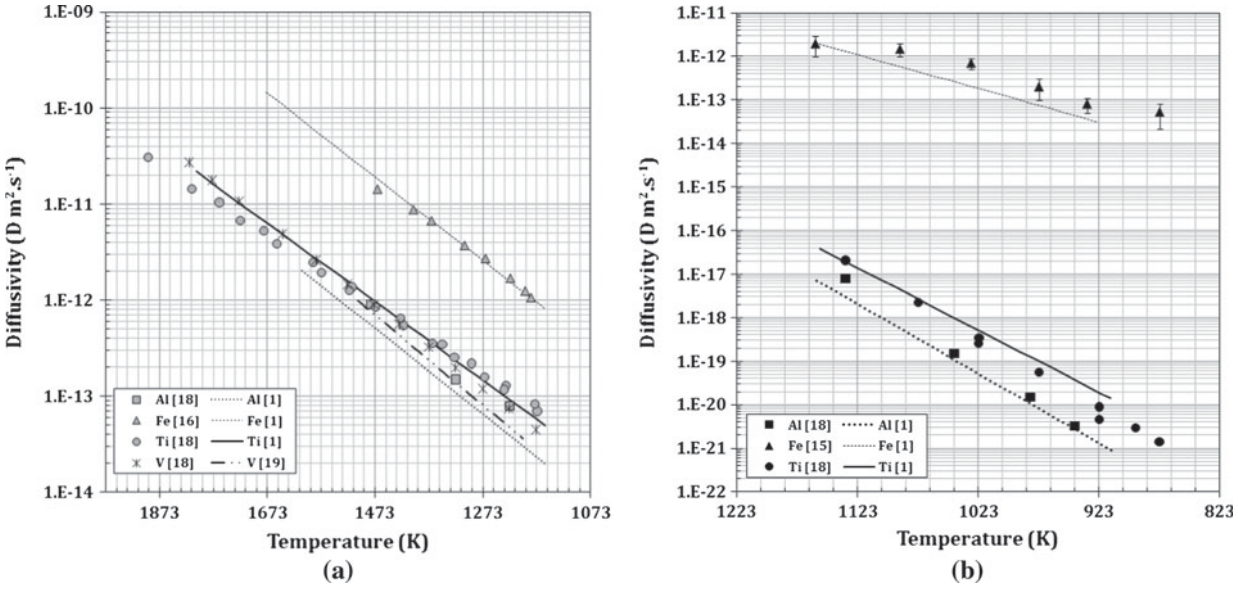

Fig. 5—Temperature dependence of diffusion coefficients for solute diffusion and self-diffusion in pure β-Ti (*a*) and α-Ti (*b*).

the final stage of dehydrogenation and was preserved during subsequent heating. A more rapid shrinkage for the Ti-1033 composition upon continuous heating leads to lower residual porosity than that of the Ti-1023 alloy (Table I). A similar result was observed in Reference 13, in which an increase in the iron content accelerated densification of Ti-Fe alloys. This can be explained by the anomalously high diffusion mobility of iron in titanium,[1,15,16] which is an order of magnitude higher than self-diffusion of titanium atoms for β lattice and five orders of magnitude higher for α lattice (Figure 5). Thus, the addition of an extra 1 pct Fe accelerates interdiffusion in powder compacts, resulting in activated sintering and lower residual porosity.

An important distinctive feature of the Ti-1033 alloy synthesis is the specific redistribution of alloying elements upon homogenization, which is different than the homogenization process for earlier studied compositions including the Ti-1023 alloy.[10] Figure 2 shows that iron penetrates the titanium matrix more actively than aluminum at the starting stage of Ti-1033 homogenization. For Ti-5Al-5V-5Mo-3Cr and Ti-1023 compositions sintered using complex master alloy powders,[10] a different sequence of alloying element redistribution was observed; homogenization started with the diffusion of aluminum in titanium, whereas Fe was ''trapped'' in the master alloy particles for a longer time. To explain this difference in the sequence of element redistribution, the diffusion mobilities of separated alloying elements (Al, Fe, and V) in titanium and their solubilities in α and β titanium phases should be taken into account. Aluminum is characterized by a noticeably lower diffusion mobility than iron in both α and β titanium (Figure 5). However, the solubility of aluminum in the α and β titanium phases is relatively high (at least 7 pct at 773 K (500 °C) with additional increases at higher temperatures), whereas the solubility of iron in the α phase is less than 0.1 pct.[17] The sequence of phase transformations upon dehydrogenation of the titanium matrix ($TiH_2 \rightarrow \beta \rightarrow \alpha$[10]) is completed by the formation of α titanium at 873 K to 923 K (600 °C to 650 °C) upon heating. The formation of the α-titanium lattice around alloying particles at these relatively low temperatures is favorable for the penetration of aluminum but creates an insuperable phase barrier for iron (and any other β-stabilizing elements) diffusion, slowing the dissolution of alloy powder particles. Such a situation, earlier observed for Ti-1023 synthesis,[10] can remain up to 1273 K to 1373 K (1000 °C to 1100 °C) and results in the retardation of homogenization. Additional increases in temperature eventually lead to the disappearance of the α-phase barriers stabilized with Al and completion of

the $\alpha \rightarrow \beta$ transformation in the surrounding titanium matrix. This process results in the fast penetration of iron followed by the slower diffusion of vanadium into the titanium. However, such retarded homogenization then leads to negative consequences such as a low relative density and excessive grain growth.[10]

The opposite scheme of element redistribution was observed for the Ti-1033 alloy in the present study. Iron penetrated into the titanium simultaneously with aluminum and even more actively than Al at early stages of heating. This suggests that an increase in the Fe/Al concentration ratio in the master alloy particles changes the equilibrium homogenization kinetics for these alloying elements. An increase in iron content with a corresponding relative decrease in Al concentration within the master alloy particles obviously reduces the negative influence of the α-phase barrier around alloying particles, presumably because of the completion of the $\alpha \rightarrow \beta$ transformation at lower temperatures. This creates favorable conditions for the accelerated penetration of iron into the titanium matrix. Under such conditions, the potential for high-diffusion mobility of iron was realized to a considerable degree even at relatively low temperatures (Step I), which led to an advanced redistribution of iron in comparison with aluminum. This phenomenon drastically changes the homogenization process for the Ti-1033 alloy in comparison with Ti-1023. Previous results showed that an advanced iron redistribution was obtained with an increase in the heating rate, which had a positive effect on the density of the final product.[10] In the present study, a similar result was achieved with an increase in the iron content. As for the third alloying element, vanadium, its diffusion rate is noticeably lower than that of Al[1,18,19] (Figure 5); resulting in its slow redistribution in titanium and delayed achievement of full chemical homogeneity for both compositions in comparison.

The variation in iron content also resulted in a difference in the grain size for the Ti-1033 and Ti-1023 compositions (Table I); the intragranular microstructure formed upon postsintering cooling and, hence, resulted in different mechanical properties. The beta grain size formed during synthesis at temperatures above the $\alpha \rightarrow \beta$ transformation usually depends on the chemical composition of the alloy (*i.e.*, diffusion mobility of elements), which determines grain boundary mobility. For materials produced by BEPM, pores in the microstructure also have a noticeable influence on the grain size because pores are effective grain boundary stoppers preventing the movement of boundaries.

The high diffusivity of iron and more active reduction in porosity with an increase in its content promoted more rapid grain growth for the Ti-1033 composition compared with Ti-1023 (Table I). Contrary to the grain size, which was formed upon synthesis in the single β-phase field, the intragranular $\alpha + \beta$ microstructure (Figure 4) was formed upon postsintering furnace cooling because of β-phase decomposition. Since the thermal stability of beta phase is affected by chemical composition, variations in the iron content also have an influence on the size of α-phase precipitates in the β matrix. Higher Fe contents increase the stability of the β phase, so its decomposition upon cooling is less developed, resulting in finer α lamellae in the Ti-1033 alloy compared with that of Ti-1023 (*cf.* Figures 4(b) and (d)).

The intragranular $\alpha + \beta$ microstructure, β grain size, and residual porosity (relative density) determine the balance of tensile mechanical properties of synthesized alloys (Table I). Differences in the intragranular microstructure are main factors that determine distinctions in mechanical properties, whereas different porosities and grain sizes emphasize the influence of intragranular structure on the material ductility. Coarse α precipitates formed in Ti-1023 are typical for the ductile condition with relatively low strength. At such strength levels, the negative effect of a residual 4 pct porosity on the ductility was negligible. For the Ti-1033 alloy, finer α precipitates resulted in a strengthened condition with a corresponding loss in ductility. Moreover, at higher strengths the negative effect of coarser grains and residual pores on the ductility became more pronounced. Thus, even despite the decrease in residual porosity, Ti-1033 demonstrated low ductility. The ductility of the Ti-1033 alloy can be improved with the formation of coarser α precipitates using either slower postsintering cooling or additional heat treatment in the $\alpha + \beta$ phase field. Additional experiments with slower postsintering cooling in the furnace resulted in improved tensile elongation (9.8 pct) at decreased strength level (YS = 949 MPa, UTS = 1059 MPa). As for the achievement of a satisfactory balance of properties in the strengthened condition, increasing the iron content to 3 pct was not sufficient. To improve ductility of Ti-1033 in the strengthened condition, additional decreases in residual porosity while maintaining a fine grain size is necessary. This could be achieved by using additional methods such as the preservation of the β-state titanium matrix during dehydrogenation with the application of a higher heating rate.[10] The application of this approach for Ti-1033 in addition to a decrease in the sintering temperature to 1473 K (1200 °C) led to reduced porosity of 3 pct at 110-μm average grain size, and improved the balance of properties after furnace cooling (YS = 1047 MPa, UTS = 1186 MPa, and El. = 4.9 pct).

V. CONCLUSIONS

The following conclusions were drawn after completing this study:

1. A homogeneous, nearly dense Ti-10V-3Fe-3Al alloy was synthesized by the BEPM approach.
2. A comparison of the synthesis processes for the Ti-1023 and Ti-1033 alloys demonstrated that increasing the iron content resulted in the following: (1) an improved densification because of the fast diffusion mobility of this element and (2) a changed sequence of alloying element penetration into the titanium matrix upon homogenization.
3. The Ti-10V-3Fe-3Al alloy is characterized by improved sintered density (lower residual porosity) but noticeable grain growth.
4. The synthesized material possessed a sufficiently high strength level but low ductility. To improve

the balance of properties in the strengthened condition, an additional decrease is necessary in residual porosity with a simultaneous preservation of finer grain size.

ACKNOWLEDGMENT

This work was partially supported by the EMI Strategic Grant and URC Small Grant, University of Wollongong, Wollongong, NSW, Australia.

REFERENCES

1. G. Lutjering and J.C. Williams: *Titanium*, 2nd ed., Springer-Verlag, Berlin Germany, 2007, p. 442.
2. F.H. Froes and D. Eylon: *Int. Mater. Rev*, 1990, vol. 35 (3), pp. 162–82.
3. V.S. Moxson, O.N. Senkov, and F.H. Froes: *Int. J. Powder Metall*, 1998, vol. 34 (5), pp. 45–53.
4. J.E. Barnes, W. Peter, and C.A. Blue: *Mater. Sci. Forum*, 2009, vols. 618–619, pp. 165–71.
5. M. Hagiwara, Y. Kaieda, Y. Kawabe, and S. Miura: *ISIJ Int.*, 1991, vol. 31 (8), pp. 922–30.
6. T. Fujita, A. Ogawa, C. Ouchi, and H. Tajima: *Mater. Sci. Eng. A*, 1996, vol. 213, pp. 148–53.
7. M. Hagiwara and S. Emura: *Mater. Sci. Eng. A*, 2003, vol. 352, pp. 85–92.
8. T. Saito, H. Takamiya, and T. Furuta: *Mater. Sci. Eng. A*, 1998, vol. 243, pp. 273–78.
9. R.R. Boyer and R.D. Briggs: *J. Mater. Eng. Perform*, 2005, vol. 14 (6), pp. 681–85.
10. O.M. Ivasishin and D.G. Savvakin: *Key Eng. Mater.*, 2010, vol. 436, pp. 113–21.
11. O.M. Ivasishin, D. Eylon, V.I. Bondarchuk, and D.G. Savvakin: *Defect Diffusion Forum*, 2008, vol. 277, pp. 177–85.
12. W. Wei, Y. Liu, K. Zhou, and B. Huang: *Powder Metall.*, 2003, vol. 46, pp. 246–50.
13. Y. Liu, L.F. Chen, H.P. Tang, C.T. Liu, B. Liu, and B.Y. Huang: *Mater. Sci. Eng. A*, 2006, vol. 418, pp. 25–35.
14. O.M. Ivasishin, D.G. Savvakin, X.O. Bondareva, and O.I. Dekhtyar: *Proc. 10th World Conf. on Titanium (2003)*, vol. 1, Wiley-Vch Verlag, Weinheim, Germany, 2004, pp. 495–502.
15. H. Nakajima, M. Koiwa, Y. Minonishi, and S. Ono: *Trans. JIM*, 1983, vol. 24, pp. 655–60.
16. R.F. Peart and D.H. Tomlin: *Acta Metall.*, 1962, vol. 10, pp. 123–34.
17. T.D. Massalski: *Binary Alloys Phase Diagrams*, Eds. H. Okamoto, P.R. Subramanian, and L. Kasprzak, ASM International, Materials Park, OH, 1990.
18. G. Neumann and C. Tuijn: *Self-diffusion and Impurity Elements Diffusion in Pure Metals: Handbook of Experimental Data*, Pergamon Materials Series, vol. 14, Elsevier, Amsterdam, The Netherlands, 2008, pp. 1–349.
19. Z. Liu and G. Welsch: *Metall. Trans. A*, 1991, vol. 22A, pp. 946–47.